UCRL-JC-126541
PREPRINT

Probing High Density Plasmas with Soft X-Ray Lasers

P. Celliers, T.W. Barbee Jr.,R. Cauble, L.B. Da Silva, C.D. Decker, D.H. Kalantar, M.H. Key, R.A. London, J.C. Moreno, R. Snavely, J.E. Trebes, A.S. Wan and F. Weber

This paper was prepared for submittal to the
Society of Photo-Optical Instrumentation Engineers
Soft X-Ray Lasers and Applications II
San Diego, CA
July 28-29, 1997

August 1997

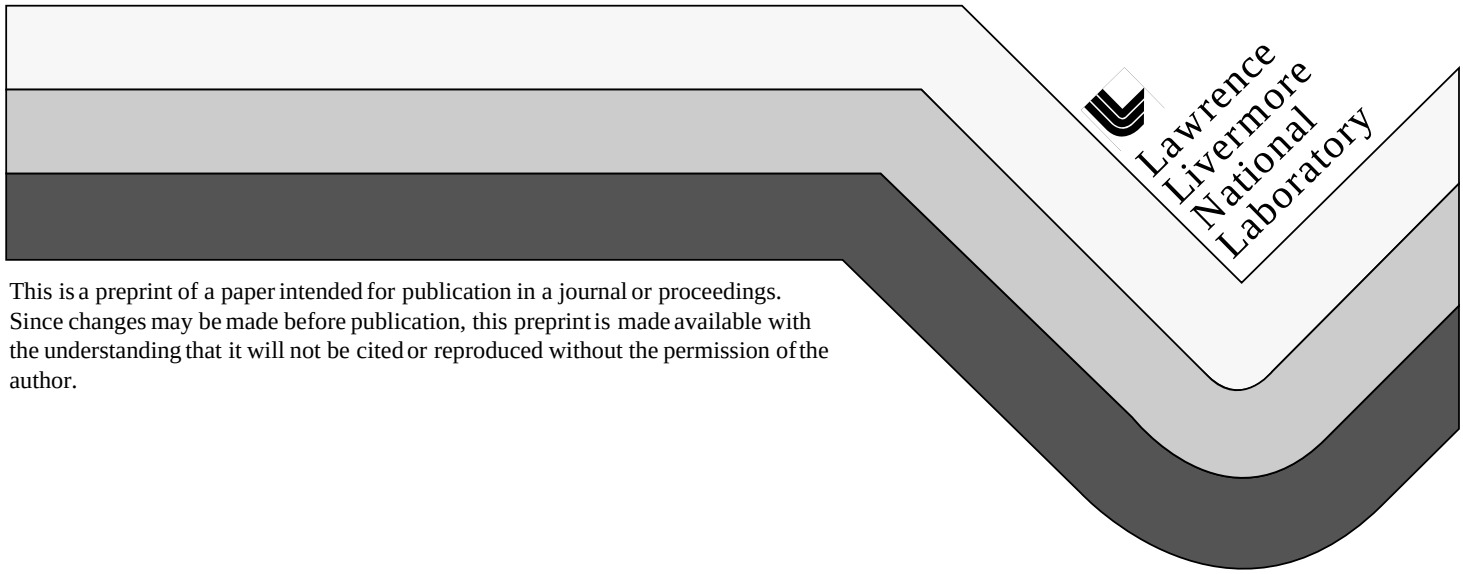

This is a preprint of a paper intended for publication in a journal or proceedings. Since changes may be made before publication, this preprint is made available with the understanding that it will not be cited or reproduced without the permission of the author.

DISCLAIMER

This document was prepared as an account of work sponsored by an agency of the United States Government. Neither the United States Government nor the University of California nor any of their employees, makes any warranty, express or implied, or assumes any legal liability or responsibility for the accuracy, completeness, or usefulness of any information, apparatus, product, or process disclosed, or represents that its use would not infringe privately owned rights. Reference herein to any specific commercial product, process, or service by trade name, trademark, manufacturer, or otherwise, does not necessarily constitute or imply its endorsement, recommendation, or favoring by the United States Government or the University of California. The views and opinions of authors expressed herein do not necessarily state or reflect those of the United States Government or the University of California, and shall not be used for advertising or product endorsement purposes.

Probing high density plasmas with soft X-ray lasers

P. Celliers, T.W. Barbee. Jr., R. Cauble, L.B. Da Silva, C.D. Decker, D.H. Kalantar, M.H. Key, R.A. London, J.C. Moreno, R. Snavely, J.E. Trebes, A.S. Wan and F. Weber

Lawrence Livermore National Laboratory, Livermore CA, 94550

Abstract

Collisionally pumped x-ray lasers are ideal for a wide variety of plasma diagnostics. They have been demonstrated over a wavelength range extending from 3.5 nm to 40 nm and have output energies as high as 10 mJ in 150 ps pulses. The beam divergence is less than 15 mrad and the linewidth $\lambda/\Delta\lambda \sim 10^4$ provides sufficient longitudinal coherence for interferometry. Using various arrangements constructed with multi-layer XUV reflective optics we have carried out a variety of experiments with the yttrium x-ray laser operating at 15.5 nm. Initial experiments involved x-ray laser backlighting and Moiré deflectometry, while later work demonstrated interferometric determinations of plasma density profiles in various targets. We have also studied hydrodynamic imprinting of laser speckle patterns on directly driven thin foils with 1-2 μm spatial resolution. These detailed plasma diagnostic capabilities provide an important means to benchmark hydrodynamic calculations of dense plasma flows.

Keywords: X-ray laser, optical probing, shadowgraphy, radiography, interferometry

2. Introduction

High density plasmas with electron densities exceeding 10^{21} cm^{-3} and scale-lengths up to several mm are readily produced with large laser systems such as the Nova laser at Lawrence Livermore National Laboratory, and at several other laboratories around the world. The high brightness and short wavelengths available with collisionally-pumped X-ray lasers has made it possible to develop optical probe diagnostics of these large plasmas. These systems have been demonstrated to operate at wavelengths ranging from 3.5 to 40 nm. Saturated output has been reported in selenium,[1] germanium[2] and yttrium[3] using optical pumping and in argon[4, 5] using capillary discharges. Initially these sytems required high energy optical laser systems to produce a hot uniform plasma suitable for amplification. Considerable recent progress has been made using more sophisticated pumping techniques[6-11] to improve the efficiency and capabilities of these systems. At the same time recent advances in optical multi-layer technology[12] has enabled construction of optical imaging systems for manipulating the soft x-ray beam as a probe source.

The experiments described in this report were all performed at the Nova two-beam laser facility, using one Nova beam to drive the x-ray laser and the other Nova beam to generate the plasma object. The x-ray laser was produced by irradiating an exploding foil 3 cm long yttrium target with one beam from Nova using a 600 ps square pulse at 0.53 μm wavelength and an intensity of 1.5×10^{14} W/cm^2. The x-ray laser had an output energy of 5-10 mJ, a divergence of approximately 10 mrad (FWHM) and an output pulse width of 80-100 ps. This system has been well characterized[3] and has proved itself robust and effective for routine operation. For plasma probing experiments the x-ray laser beam was usually relayed by several Mo/Si multilayer mirrors: in most cases we used a 1 m radius spherical mirror to collimate the beam and another 1 m radius spherical mirror as an imaging optic. All multilayer mirrors consisted of 15-30 layer pairs of Mo/Si deposited on a superpolished (< 0.1 pm roughness) fused silica substrate and had a measured reflectivity of 60±5 % at normal incidence. The effective bandpass of the multilayer mirror optical system was 0.8 nm centered at 15.5 nm. Depending on the particular experiment other multi-layer optics were often used for additional beam manipulations. For most experiments we recorded images with a CCD detector (a back illuminated TEK1024B with 1024 by 1024 24 μm pixels) with a measured quantum efficiency of 40±10% at 15.5 nm. Optical and UV light was blocked by a 100 nm aluminum filter placed in front of the CCD. The high brightness of the XUV laser combined with the narrow bandpass of the optical system and the filtering allowed us to record clean images with negligible background using this time-integrating detector.

In section 3 we discuss optical probing issues for high density plasmas and describe the main advantages of XUV sources for this purpose. Section 4 reviews a couple of examples of using the x-ray laser probes as a simple backlighter for shadowgraphy and radiography. Section 5 reviews the use of the x-ray laser for electron density measurements of laser-produced plasmas using interferometry. Conclusions and expectations for future developments are presented in Section 6.

3. Optical probing of high density plasmas

Optical probing techniques are often used to study plasmas, transparent fluids and transparent solids. Two-dimensional imaging techniques of varying complexity include shadowgraphy, deflectometry (or schlieren and related methods) and interferometry. All are widely used in many applications because they can provide a rich level of detail. Generally the fluid disturbance or plasma flow under study appears as a transparent and weakly refracting object to the probe beam. One encounters limitations in using visible and near UV wavelengths for direct optical probing of large laser-produced plasmas mainly because these plasmas exhibit both strong absorption and strong refraction at the conventional probe wavelengths. Often the regions of interest are not weakly refracting, they can be opaque and they may contain a critical density layer which does not produce small perturbations on the probe beam. As we discuss below, both absorption and refraction of optical beams are greatly reduced when the wavelength of the probe beam is reduced, and the critical density surface is eliminated. This is the principal advantage to the use soft x-ray or extreme

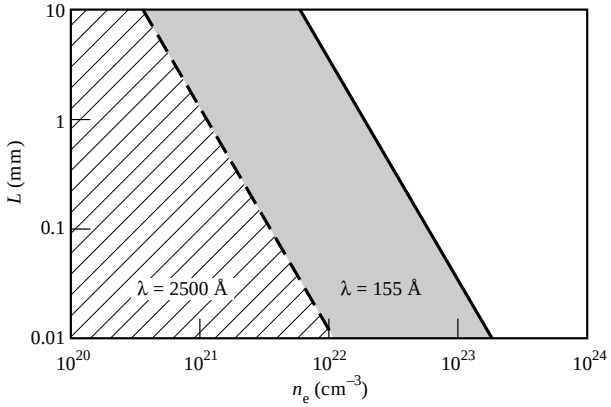

Figure 1. Parameter space accessible for plasma probing using an optical laser (250 nm) and a soft x-ray laser (15.5 nm). Only bremsstrahlung absorption is considered.

ultra-violet (XUV) sources for probing these plasma flows. However, even at the much shorter XUV wavelengths absorption and refraction must be considered, because they place the ultimate limits on the size or density of plasma that can be probed. Absorption places limits primarily on the maximum density of the plasma, while refraction places limits on the the magnitude of density gradients that can be tolerated.

One can estimate the constaint imposed by absorption through considering only bremsstrahlung opacities which is usually the single dominant absorption mechanism. For most high temperature plasmas of interest, the level of ionization is sufficient to eliminate any bound-free absorption in the soft x-ray region. Resonant line absorption is possible but very unlikely given the narrow bandwidth[13] of the x-ray laser ~1 pm. The bremsstrahlung absorption coefficient, α, is approximately given by[14]

$$\alpha = 2.42\times10^{-37}\,\frac{\langle Z^2\rangle n_e n_i}{\sqrt{T_e}\,(h\nu)^3}\left[1-\exp(-h\nu/kT_e)\right] \qquad (1)$$

where , α, is in cm^{-1} the electron temperature, T_e, and photon energy, $h\nu$, are in eV and electron density n_e and ion density n_i are in cm^{-3}. The strong scaling with photon energy ($\propto \nu^{-2}$ when $h\nu << kT_e$) shows the advantage of probing with XUV sources. Therefore, if we consider only bremsstrahlung absorption in a plasma with 1 keV temperature and average ionization 30 (mid-Z plasma) we obtain from equation (1), $\alpha \approx 3.6\times10^{-44} n_e^2$ for λ=15.5 nm. If we allow for one optical depth (i.e. $\alpha L = 1$) of absorption we obtain $n_e^2 L = 2.8\times10^{43}$. In Figure 1 we compare the

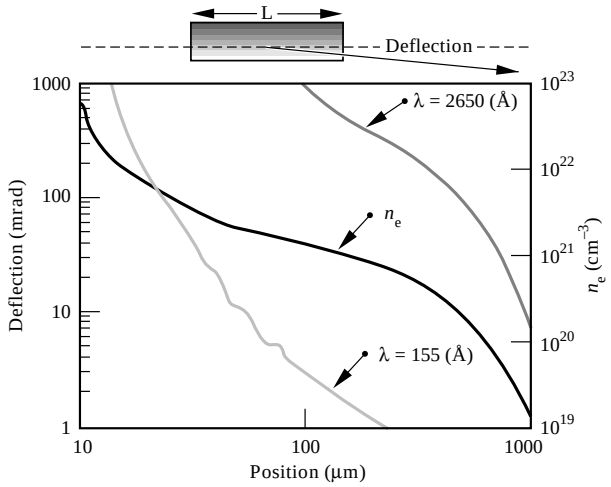

Figure 2. Calculated density and deflection for an optical and an x-ray laser probe traversing 3 mm of plasma produced by driving a 50-μm thick CH target with a 1-ns square 0.53 μm laser pulse at 2.0×10^{13} W/cm^2.

electron density and plasma dimension accessible with a XUV laser source (15.5 nm) and a conventional UV laser source (250 nm). The strong wavelength scaling ($\propto \lambda^2$) makes it a clear advantage to probe with shorter wavelengths. The possible parameter space with a 15.5 nm probe easily covers the plasmas normally produced in the laboratory.

Refraction of the probe beam is sensitive to electron density gradients and ultimately affects spatial resolution and data interpretation. At 15.5 nm critical density is 4.6×10^{24} cm^{-3} which is well above the densities of most plasmas of interest. For a simple plasma with a linear density gradient $n_e = n_o\left[1-(y / y_o)\right]$, the deflection angle, θ, scales as $\theta \propto \lambda^2 L / y_o$. This strong scaling again makes it advantageous to use a short wavelength probe. In Figure 2 we compare the deflection angle after propagating through a 3 mm plasma for an optical (265 nm) and XUV (15.5 nm) probe source. At a fundamental level large deflection angles imply significant spatial blurring, reduced spatial resolution and the need for a fast imaging optic. For example, a 10 mrad deflection angle leads to 10 μm translation over a 1 mm long plasma. Light deflected by more than 25 mrad will not be collected by a f/20 imaging optic. In addition, since probe rays propagate through a range of electron densities interpretation of the results is more difficult for large deflections.[15]

4. Shadowgraphy and radiography

Shadowgraphy with an XUV laser illumination source is the least demanding type of diagnostic, and requires a simple arrangement involving only a single spherical mirror operating at near normal incidence. Micron scale resolutions are easily obtained even using a relatively slow f/20 imaging optic, owing to the short wavelength of the source. An example of a high resolution shadowgraph of a thin laser-accelerated foil is shown in Figure 3. The target, a 3 μm Al foil coated with a 10 μm CH ablator, was accelerated by a 1 ns, 0.53 μm Nova beam focused to 10^{14} W/cm^2. The image in Figure 3 was recorded 1.1 ns after the start of the drive pulse. The drive beam was smoothed with an arrangement consisting of a random phase plate and a segmented array of wedges to produce a flat-top intensity distribution over a 0.7 mm diameter spot.[16] The short wavelength of the XUV probe allows one to obtain micron-scale spatial resolution of the high density plasma close to the rear surface of the accelerated foil. Clearly visible in the recorded image are micron scale non-uniformities produced in the rear side of the accelerated and expanded aluminum. The information available in this data is limited, because it is difficult to infer a density profile or obtain a complete picture of the non-uniformities since the viewing direction was transverse to the foil. Nevertheless the conclusion obtained from these early studies was that the non-uniformities produced on the rear surface were seeded by early time imprinting of laser speckle from the smoothed drive beam. The amplitudes of non-uniformities were subject to Rayleigh-Taylor growth during the foil acceleration. More details of this work has been previously reported[17] and demonstrated the potential of high resolution imaging with simple spherical multilayer mirrors.

Unambiguous quantitative analysis of the results shown in Figure 3 is not possible owing to incomplete knowledge of the density profile, and due to the side-on viewing geometry. However the effects of imprinting and subsequent Rayleigh-Taylor growth are amenable to far more precise and quantitative study once again using the XUV laser source in another experimental variation, this time using a viewing geometry that allows face-on radiography of the laser-accelerated foil. The observable of interest in this case is the areal density of the accelerating foil which can both be measured directly and modeled with two- or three-dimensional simulation codes. The potential of XUV lasers

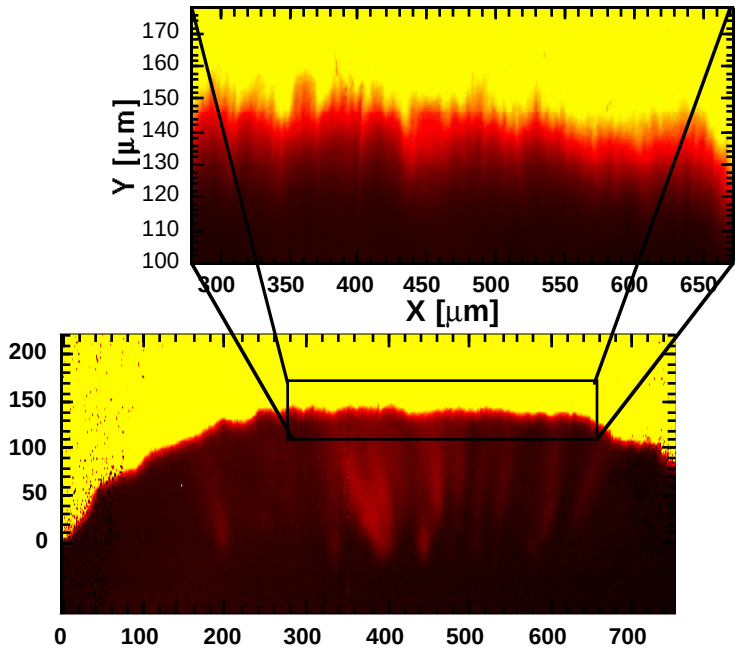

Figure 3. Side on XUV radiograph of a foil (10 μm CH on 3 μm Al) accelerated by a 1 ns Nova pulse recorded at 1.1 ns after the beginning of the drive pulse. The foil was originally positioned at zero on the vertical scale.

for studying this problem was first described by Key[18] and the initial demonstrations were performed at the Nova two-beam facility by Kalantar et al.[19] Later studies using a Ge XUV laser to backlight accelerated Al foils were carried out at the Vulcan laser in a larger international collaboration.[20] In studying this effect it is important to maximize the experimental sensitivity to target modulations so that measurements can be made early in the pulse before Rayleigh-Taylor growth has dominated. It is easy to show that the sensitivity is maximized when one uses a target with a large optical depth[18] which then requires the use of a bright probe. For example the 3 μm Si sample used in the initial experiments had an optical depth of 6.5 (attenuation of approximately 700), which produces a 10% modulation in the detected intensity for a 50 nm modulation in the local thickness of the target. Thus, it is powerful means to examine the initial imprint of small amplitude non-uniformities.

The experimental setup used for these experiments is shown in Figure 4. In this experiment 3-4 μm Si foils are irradiated at 3×10^{12} W/cm^2 with a 0.5 ns square, 0.35μm wavelength beam from the Nova laser. The driven foil is imaged with a spherical mirror (50 cm radius of curvature) onto a backthinned CCD detector. An additional flat mirror was used after the imaging optic to further reduce the bandpass of the system. The spatial resolution of this imaging system has been measured to be ~ 1μm and is limited by the CCD detector pixel size of 24 μm and spherical aberrations in the imaging system. The streak camera and second CCD camera were used to monitor the quality and timing of the XUV laser beam.

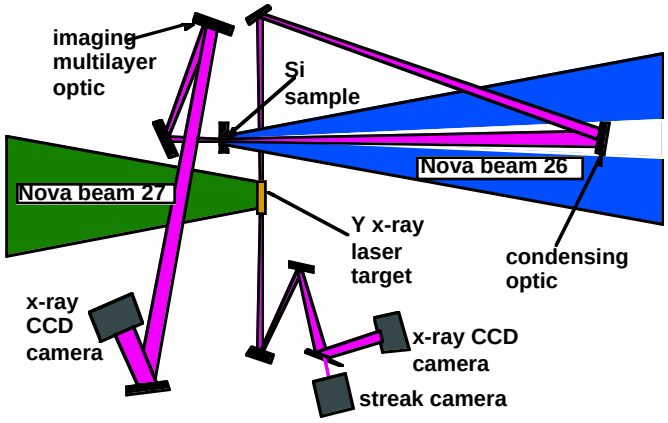

Figure 4. Experimental setup used to study laser imprinting using soft x-ray imaging.

In Figure 5 we show the recorded image for three different irradiation conditions all employing a smoothing by spectral dispersion[21] (SSD) scheme to impose temporal and spatial modulations on the speckle pattern in the focal spot of the drive laser. Various levels of the modulation frequency bandwidth were investigated. Figure 5(a) and (b) was taken 260 ps after start of the laser pulse to coincide with the breakout of the shock at the rear surface while Figure 5(c) was taken at 400 ps after an interval of Rayleigh-Taylor growth. Figure 5(a) was obtained with a laser beam with no bandwidth whereas 5(b) and 5(c) used a cross phase modulated beam with bandwidth of 1.4 Å (0.33 THz). The measured RMS optical modulations for images in Figure 5(a),(b) and (c) are 0.37, 0.22, and 0.58 respectively. The benefits of SSD and increased bandwidth are evident in the reduction in optical depth modulations of the imprint relative to the static speckle pattern. More details of this work and a comparison to model predictions can be found in the works by Kalantar et al.[19, 20, 22]

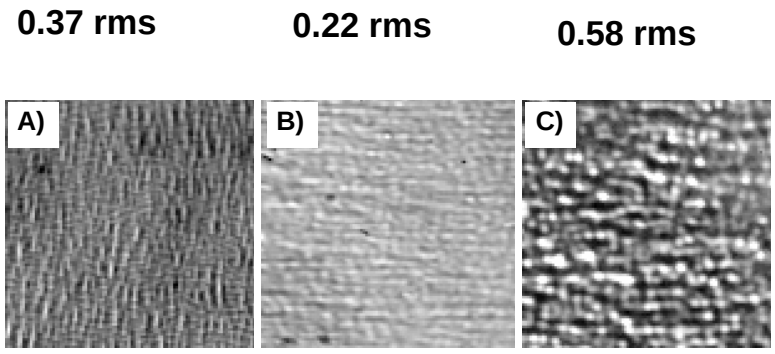

Figure 5. Images obtained of laser irradiated thin silicon foils. Image a) and b) were obtained 260 ps while image c) was 400 ps after the start of the drive. Image a) used a laser beam with no bandwidth. Image b) and c) used a laser beam with 1.4 Å bandwidth. The measured RMS optical depth modulations of these images is shown.

5. Electron density measurement

Spatial variations in electron density of a plasma object produce variations in refractive index, which can be studied using methods sensitive directly to the refractive index (interferometry) or to gradients in the refractive index (schlieren techniques and deflectometry). In all cases these techniques place more stringent demands on the coherence properties of the illumination source than in the case of shadowgraphy. The high brightness (i.e. strong collimation) and coherence of the XUV beam make all of these techniques possible. Moiré deflectometry is a means

of obtaining quantitative information on density gradients in a sample. It requires a highly collimated illumination but the experimental arrangement is not much more demanding than a shadowgraphy arrangement. For these reasons our initial measurements of electron density profiles in laser produced plasmas were obtained using Moiré deflectometry.[23] The technique is somewhat limiting, because it produces a signal proportional to the electron density gradient along only one dimension. However, its simplicity continues to have clear advantages; further demonstrations of this technique are reported in these proceedings.[24] Interferometry has the advantage of providing much more detail on electron density profiles in plasmas since it yields a two-dimensional map of the electron density in the plasma. In the study of laser produced plasmas optical interferometry has played a key role in the accurate measurement of electron density profiles for a variety of target conditions. Profile steepening due to radiation pressure was first quantified by Attwood et al.[25] using a short pulse 265 nm optical interferometer. It has been used to measure electron density profiles in exploding foils under conditions relevant to x-ray lasers.[15] The filamentation instability in laser produced plasmas was investigated by Young et al.[26, 27] also using optical interferometry. In all these cases, however, the size of the plasma and the peak electron density accessible were severely restricted by absorption and refraction. For these reasons there has existed a need to develop techniques operating at soft x-ray wavelengths where absorption and refraction effects can be mitigated.

In a plasma with electron density n_e, the index of refraction, n is related to the critical electron density, $n_{cr} = 1.1\times10^{21}\lambda^{-2}$ (n_{cr} in cm^{-3}, λ in μm), by $n = \left[1 - n_e / n_{cr}\right]^{1/2} \approx 1 - n_e / 2n_{cr}$. The fringe shift observable in an interferogram is given by,

$$\Delta\Phi = \int_0^L \frac{\delta n}{\lambda} dx = \frac{L}{2\lambda}\frac{n_e}{n_{cr}},$$

where L is the path length through the plasma along which the beam propagates. The fringe shift can be evaluated directly over the entire two-dimensional field of the interferogram, and yield in turn the electron density directly as long as L is well defined. However, interferometry demands an arrangement that is more complicated and is potentially difficult to execute given the limited coherence of the XUV lasers.

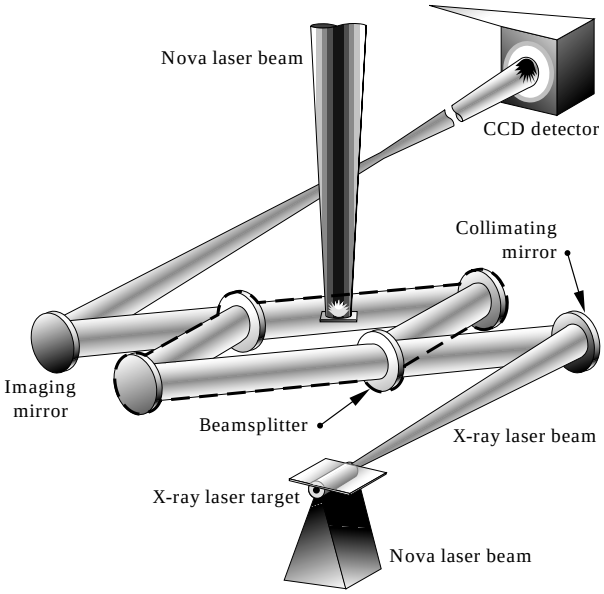

Figure 6. Experimental setup showing the components for plasma probing using a soft x-ray interferometer.

The experimental setup used to probe plasmas is shown schematically in Figure 6. The system consists of a collimated x-ray laser source, an imaging mirror and an interferometer. For our experiments we employed a Mach-Zehnder interferometer consisting of 2 flat multilayer mirrors and 2 multilayer beamsplitters operating at near-normal incidence. The beamsplitters used in the interferometer are the most critical element of the system. Soft x-ray beamsplitters with small apertures have been previously used in x-ray laser cavities[28] but comparatively large open

areas were necessary for our application. The clear aperture of the beamsplitters used in the interferometer was 1.2 cm x 1.2 cm and consisted of 100 nm of silicon nitride overcoated with 8 to 12 layer pairs of Mo/Si. The beamsplitters were fabricated from polished silicon wafers overcoated with 100 nm of silicon nitride. The silicon substrate thickness

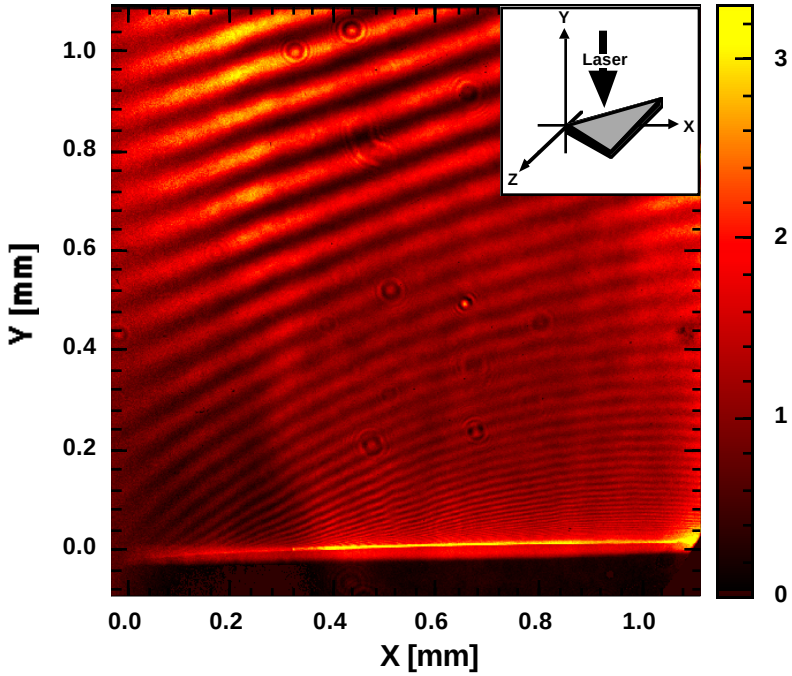

Figure 7. Interferogram of CH target irradiated at 2.7×10^{13} W/cm^2. The inset shows the target geometry.

was varied from 0.4 - 0.8 mm with the best results being achieved with the thicker samples. The coated wafers were annealed to achieve maximum tension in the silicon nitride. Anisotropic silicon etching techniques were used to remove the silicon substrate from a 1.2 cm x 1.2 cm area. The flatness of the beamsplitters was subsequently measured with an optical interferometer. Over the clear aperture the flatness was typically better than 500 nm for high quality silicon substrates but could be significantly worse (1000 nm) for conventional thin (0.4 mm) silicon wafers. The figure quality was also extremely sensitive to the tension of the silicon nitride membrane. The best results were obtained with high stress membranes (~200 MPa) which had a fabrication yield of approximately 30%. The measured reflectivity and transmission for these beamsplitters at 15.5 nm was 20% and 15% respectively. The overall throughput of each arm, accounting for the mirror and beamsplitter (one transmission and one reflection), was ~ 0.018.

Alignment tolerances of the interferometer were dictated by the coherence properties of the illumination beam. The transverse coherence length after beam collimation was estimated to be $L_s \approx 50 - 100\,\mu$m and the longitudinal coherence length was measured[29] to be $L_t \approx 150$ μm. The interferometer was pre-aligned on an optical bench using a 100 μm optical fiber and a white light source. Observation of white light fringes was used to match the optical path lengths to better than 2 μm. Furthermore, overlap of the signal and reference beams was carefully adjusted to match better than 50 μm at the object plane. The plasma to be probed was imaged onto a CCD with a 100 cm radius of curvature multilayer mirror with an effective focal ratio of f/25. To reduce background self-emission a series of 3 multilayer mirrors were used to narrow the bandpass of 0.4 nm, which is significantly broader than the 1 pm spectral width of the x-ray laser source. The image magnification was 19 giving a pixel limited resolution of ~1.3 μm.

In Figure 7 we show the interferogram of a plasma produced by irradiating a silicon wafer overcoated with 10μm of CH. The target was in the shape of a triangle to allow a range of plasma lengths to be probed simultaneously. The silicon substrate was polished to ~0.7 nm rms roughness to produce a clean flat surface. The CH side was irradiated with a beam smoothed with same random phase plate and segmented wedges focusing scheme as used in the experiment of Figure 3. A 1 ns square laser pulse with a wavelength of 0.53 μm produced an intensity on target of 2.7×10^{13} W/cm^2. The target was illuminated from the side by the x-ray laser beam 1.1 ns after the start of the laser pulse. The image shows excellent fringe visibility and very little self emission from the plasma. This interferogram was analyzed and compared to simulations in a recent work by Da Silva et al.[30]

More recently we have used this interferometer to probe colliding plasmas which have relevance in inertial confinement fusion (ICF) hohlraum experiments. Colliding plasma experiments are motivated by the need to understand plasma interpenetration at the collision zone. Single-fluid Langrangian hydrodynamic codes used typically for ICF design work do not account for the effects plasma interpenetration. Without allowance for interpenetration the fluid elements collide and stagnate at the collision point, thus converting their kinetic energy to internal energy. The result is an unphysically large predicted ion temperature, as well as the production of strong shocks that propagate away from the collision zone. Furthermore, in some situations single fluid codes can also predict high velocity plasma jets or streaming plasmas, which are caused by related mechanisms.

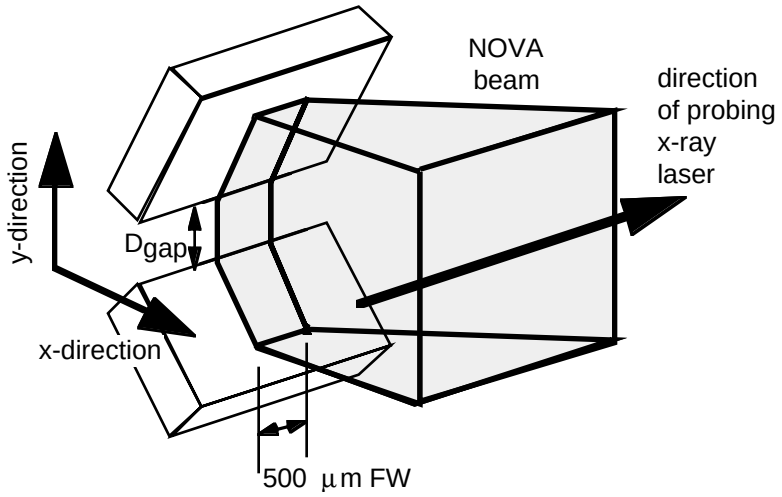

Figure 8. Three-dimensional view of the experimental configuration for the colliding plasma experiment, with x- and y-axis definitions indicated.

We investigated colliding plasma dynamics using a target geometry consisting of two pieces of polished silicon 3 mm by 2 mm that were coated with 2 μm of gold. The pieces were oriented at right angles and positioned as shown in Figure 8 with a gap between the inside edges. The target was irradiated with a 1 ns square laser pulse at an intensity of 3×10^{14} W/cm^2, and 0.53 μm wavelength. The focal spot was 2 mm high and 0.5 mm wide and was produced by combining a cylinder lens and a random phase plate.[16] The interferogram shown in Figure 9 was obtained at a time 1.0 ns after the start of the drive. There is clear evidence of plasma interpenetration and collision.

Figure10(a) shows several electron density curves obtained at the central region of plasma collision, for three different experiments recorded at different times and/or gap spacings. The experimental results showed clearly that when the collisionality is low enough (earlier time or larger gap) the counterstreaming plasmas interpenetrate significantly without developing a density maximum in the symmetry plane. The fluid-like collision does not develop until the size of the interpenetrating region approaches the size of the collision mean free path: in our case the region of plasma stagnation and interpenetration was ~ 100μm which is larger than predicted by single fluid codes which neglect interpenetration. The 100 μm interpenetration size is, however, consistent with the ion-ion collision mean free path in the collision zone. A comparison of experimental density profiles obtained from three experiments is compared with LASNEX simulations in Figure 10(b). The LASNEX calculations clearly show a much stronger density maximum than we observed experimentally. For further details of these experiments refer to the work by Wan et al.[31]

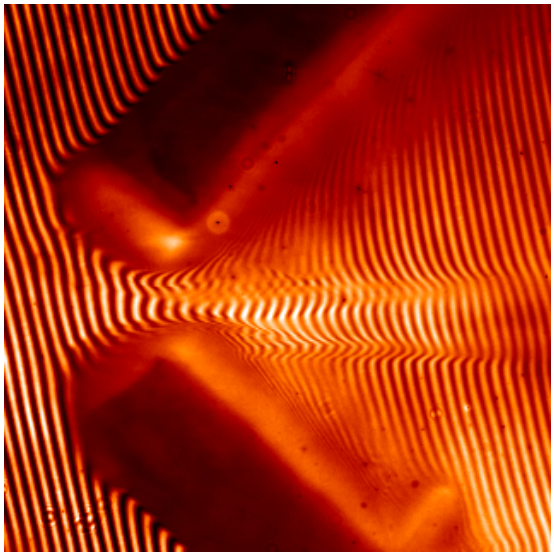

Figure 9. Interferogram of two colliding gold plasmas in the center of a 250 μm gap target probed at 1.0 ns after the beginning of the laser pulse.

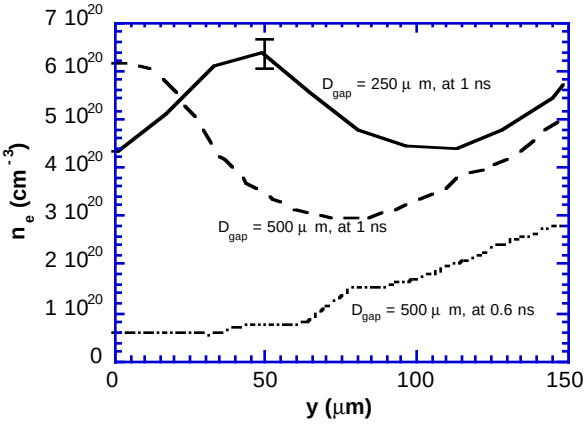

(a)

(b)

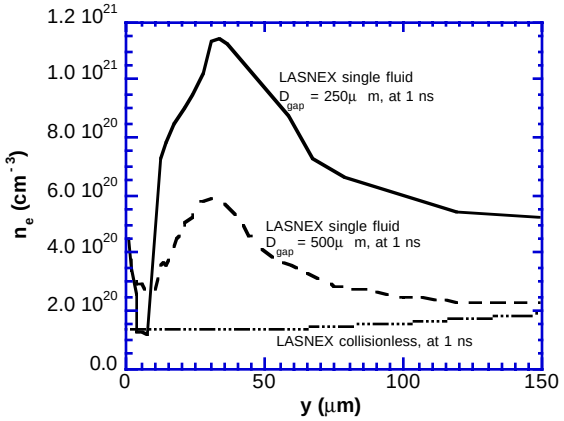

Figure 10. Comparison of (a) experimentally measured electron density profiles in the collision zone with (b) predictions from LASNEX. The two LASNEX single fluid predictions tend to overestimate the density. In (b) a LASNEX calculation which allows the two streams to interpenetrate (labelled collisionless) does not show a density maximum.

6. Conclusions

The high brightness, and short wavelength of XUV lasers make them ideal for probing large high density plasmas such as produced with current large laser facilities. Furthermore, these XUV sources are sufficiently coherent to allow interferometric imaging which can be used to produce detailed electron density measurements. We have demonstrated these capabilities using the yttrium XUV laser at the Nova two-beam facility. Recent developments at other laboratories around the world have demonstrated high efficiency XUV sources using much smaller drivers, and should lead to much more general general availability of these probing capabilities in other laboratories.

7. Acknowledgments

We would like to thank the Nova experiments group for their assistance in these experiments. This work was performed under the auspices of the U.S. Department of Energy at Lawrence Livermore National Laboratory under contract W-7405-ENG-48.

7. References

1. B. J. MacGowan, L. B. Da Silva, D. J. Fields, C. J. Keane, J. A. Koch, R. A. London, D. L. Matthews, S. Maxon, S. Mrowka, A. L. Osterheld, J. H. Scofield, G. Shimkaveg, J. E. Trebes and R. S. Walling, *Phys. Fluids*, **B 4**, 2326-2337 (1992).

2. A. Carillon, H. Z. Chen, P. Dhez, L. Dwivedi, J. Jacoby, P. Jaegle, G. Jamelot, J. Zhang, M. H. Key, A. Kidd, A. Klisnick, R. Kodama, J. Krishnan, C. L. S. Lewis, D. Neely, P. Norreys, D. O'Neill, G. J. Pert, S. A. Ramsden, J. P. Raucourt, G. J. Tallents and J. Uhomoibhi, *Phys. Rev. Lett.*, **68**, 2917-2920 (1992).

3. L. B. Da Silva, B. J. MacGowan, S. Mrowka, J. A. Koch, R. A. London, D. L. Matthews and J. H. Underwood, *Opt. Lett.*, **18**, 1174-1176 (1993).

4. J. J. Rocca, V. Shlyaptsev, F. G. Tomasel, O. D. Cortazar, D. Hartshorn and J. L. A. Chilla, *Phys. Rev. Lett.*, **73**, 2192-2195 (1994).

5. J. J. Rocca, V. Shlyaptsev, F. G. Tomasel, O. D. Cortazar, D. Hartshorn and J. L. A. Chilla, *Phys. Rev. Lett.*, **75**, 1236 (1995).

6. L. B. Da Silva, R. Cauble, G. Frieders, J. A. Koch, B. J. MacGowan, D. L. Matthews, S. Mrowka, D. Ress, J. E. Trebes and T. L. Weiland in *Ultrashort Wavelength Lasers II*, 158-164 (SPIE Proc. **2012,** 1993)

7. H. Daido, R. Kodama, K. Murai, G. Yuan, M. Takagi, Y. Kato, I. W. Choi and C. H. Nam, *Opt. Lett.*, **20**, 61-63 (1995).

8. P. V. Nickles, V. N. Shlyaptsev, M. Kalashnikov, M. Schnurer, I. Will and W. Sandner, *Phys. Rev. Lett.*, **78**, 2748-2751 (1997).

9. J. Nilsen, Y. Li, P. Lu, J. C. Moreno and E. E. Fill, *Opt. Commun.*, **124**, 287-291 (1996).

10. B. Rus, A. Carillon, P. Dhez, P. Jaegle, G. Jamelot, A. Klisnick, M. Nantel and P. Zeitoun, *Phys. Rev.*, **A 55**, 3858-3873 (1997).

11. J. Zhang, A. G. MacPhee, J. Lin, E. Wolfrum, R. Smith, C. Danson, M. H. Key, C. L. S. Lewis, D. Neely, J. Nilsen, G. J. Pert, G. J. Tallents and J. S. Wark, *Science*, **276**, 1097-1100 (1997).

12. T. W. Barbee, Jr., J. C. Rife, Hunter, W.R., M. P. Kowalski and a. others, *Applied Optics*, **32**, 4852-4854 (1993).

13. J. A. Koch, B. J. MacGowan, L. B. Da Silva, D. L. Matthews, J. H. Underwood, P. J. Batson and S. Mrowka, *Phys. Rev. Lett.*, **68**, 3291 (1992).

14. Y. B. Zel'dovich and Y. P. Raizer. *Physics of shock waves and high temperature hydrodynamic phenomena* (Academic Press, New York, 1966).

15. M. K. Prasad, K. G. Estabrook, J. A. Harte, R. S. Craxton, R. A. Bosch, G. E. Busch and J. S. Kollin, *Phys. Fluids*, **B 4**, 1569-1575 (1992).

16. S. G. Glendinning, S. V. Weber, P. Bell, L. B. Da Silva, S. N. Dixit, M. A. Henesian, D. R. Kania, J. D. Kilkenny, H. T. Powell, R. J. Wallace and P. J. Wegner, *Phys. Rev. Lett.*, **69**, 1201-1204 (1992).

17. R. Cauble, L. B. Da Silva, J. T.W. Barbee, P. Celliers, J. C. Moreno and A. S. Wan, *Phys. Rev. Lett.*, **74**, 3816-3819 (1995).

18. M. H. Key, J. T.W. Barbee, L. B. Da Silva, S. G. Glendinning, D. H. Kalantar, S. J. Rose and S. V. Weber, *J. Quant. Spectrosc. Radiat. Transfer*, **54**, 221-226 (1995).

19. D. H. Kalantar, M. H. Key, L. B. Da Silva, S. G. Glendinning, J. P. Knauer, B. A. Remington, F. Weber and S. V. Weber, *Phys. Rev. Lett.*, **76**, 3574-3577 (1996).

20. D. H. Kalantar, L. B. Da Silva, S. G. Glendinning, B. A. Remington, F. Weber, S. V. Weber, M. H. Key, N. S. Kim, D. Neely, E. Wolfrum, J. Zhang, J. S. Wark, A. Demir, J. Lin, R. Smith, G. J. Tallents, C. L. S. Lewis, A. MacPhee, J. Warwick and J. P. Knauer, *Rev. Sci. Instrum.*, **68**, 802-805 (1997).

21. S. Skupsky, R. W. Short, T. Kessler, R. S. Craxton, S. Letzring and J. M. Soures, *J. Appl. Phys.*, **66**, 3456-3462 (1989).

22. D. H. Kalantar, J. T.W. Barbee, L. B. Da Silva, S. G. Glendinning, F. Weber, S. V. Weber, M. H. Key and J. P. Knauer, *Rev. Sci. Instrum.*, **67**, 781-785 (1996).

23. D. Ress, L. B. Da Silva, R. A. London, J. E. Trebes, S. Mrowka, R. J. Procassini, J. T.W. Barbee and D. E. Lehr, *Science*, **265**, 514-517 (1994).

24. F. Weber, J. T.W. Barbee, P. M. Celliers, L. B. Da Silva, K. Tanaka, R. Kodama and K. Takahashi in *Soft X-ray Lasers and Applications II*, these proceedings (SPIE Proc. **3156,** 1997)

25. D. T. Attwood, D. W. Sweeney, J. M. Auerbach and P. H. Y. Lee, *Phys. Rev. Lett.*, **40**, 184-187 (1978).

26. S. Wilks, P. E. Young, J. Hammer, M. Tabak and W. L. Kruer, *Phys. Rev. Lett.*, **73**, 2994-2997 (1994).

27. P. E. Young, *Phys. Fluids*, **B 3**, 2331-2336 (1991).

28. A. M. Hawryluk, N. M. Ceglio, D. G. Stearns, K. Danzmann, M. Kühne, P. Müller and B. Wende in *Multilayer structures and Laboratory X-ray laser research*, 81-90 (SPIE Proc. **688,** 1986)

29. P. Celliers, F. Weber, L. B. Da Silva, J. T.W. Barbee, R. Cauble, A. S. Wan and J. C. Moreno, *Opt. Lett.*, **20**, 1907-1909 (1995).

30. L. B. Da Silva, J. T.W. Barbee, R. Cauble, P. Celliers, D. Ciarlo, S. Libby, R. A. London, D. Matthews, S. Mrowka, J. C. Moreno, D. Ress, J. E. Trebes, A. S. Wan and F. Weber, *Phys. Rev. Lett.*, **74**, 3991-3994 (1995).

31. A. S. Wan, J. T.W. Barbee, R. Cauble, P. Celliers, L. B. Da Silva, J. C. Moreno, P. W. Rambo, G. F. Stone, J. E. Trebes and F. Weber, *Phys. Rev.*, **E 55**, 6293-6296 (1997).